Phys Chem Minerals
DOI 10.1007/s00269-015-0768-3

ORIGINAL PAPER

Structural iron in dioctahedral and trioctahedral smectites: a polarized XAS study

N. Finck[1] · M. L. Schlegel[2] · A. Bauer[1]

Received: 2 March 2015 / Accepted: 28 July 2015

Abstract The chemical form of structural Fe in smectites influences many physicochemical properties of these clay minerals. Powder EXAFS data for structural Fe in smectites have been reported; however, the preferred orientation of clay platelets with respect to the X-ray beam may lead to erroneous conclusions on the local chemical environment. Dioctahedral montmorillonite and for the first time trioctahedral hectorite were prepared as textured samples, and the Fe local environment was probed by analysis of the X-ray absorption pre-edge peaks at the magic angle and by polarized EXAFS (P-EXAFS) spectroscopy. Compared to powder measurements, overlapping contributions from shells with distinct orientations can be filtered more easily by P-EXAFS, thus decreasing uncertainties on structural parameters. The pre-edge spectrum of montmorillonite is similar to spectra commonly reported for dioctahedral smectites. In contrast, the pre-edge spectrum of hectorite is notably distinct and hints to either differences in the site symmetry and/or in covalence. In both smectites, Fe is surrounded by a first O shell at a distance consistent with six-fold-coordinated Fe(III), suggesting that Fe(III) is located in the smectite octahedral sheet. This is corroborated by the distances and orientations of neighboring cationic shells, such as in-plane (Mg, Al) and out-of-plane Si shells. For montmorillonite, the results indicate Fe substitution for Al/Mg in the octahedral sheet, and a number of Fe neighbors consistent with random distribution in the octahedral sheet. For hectorite, results indicate a slight tendency for Fe atoms to form pairs in octahedral sheets; however, low numbers of neighboring cations were obtained, presumably a consequence of the presence of vacancies and/or Li in the vicinity of Fe, or of the coexistence of Fe and Mg neighbors with mutually canceling EXAFS waves. Consistent with pre-edge data, the coordination numbers can also indicate some incoherency in Fe-cation interatomic distances in hectorite as a consequence of site distortion. These results suggest that Fe^{3+} in hectorite locally distorts the structure of the trioctahedral phyllosilicate and tends to aggregate charge-deficient (i.e., vacant or Li^{+}-containing) octahedral sites.

Keywords Montmorillonite · Hectorite · Iron · Polarized XAS

Introduction

Smectites are widespread clay minerals forming under surface and subsurface conditions (Meunier 2005) and widely occur in weathering formations and sediments (Güven 1988). These small, flat minerals possess a large surface area and permanent layer charge. As a consequence, they can absorb and retain a variety of ions or molecules and thus they dominate the physicochemical properties in the systems in which they are present. Their high reactivity has also spurred important industrial applications such as catalysis (e.g., Güven 2009; Swarnakar et al. 1996) and health (Williams et al. 2009). Smectites are also constituents of bentonites and confer to these materials cost-efficient mechanical, hydraulic and chemical properties. Bentonites are extensively used as constituents of engineered barriers

✉ N. Finck
nicolas.finck@kit.edu

[1] Institute for Nuclear Waste Disposal (INE), Karlsruhe Institute of Technology (KIT), P.O. Box 3640, 76021 Karlsruhe, Germany

[2] CEA Saclay, DEN/DPC/SEARS/LISL, Building 391, 91191 Gif-Sur-Yvette, France

Journal : Large 269 | Dispatch : 7-8-2015 | Pages : 13
Article No : 768 | ☐ LE | ☐ TYPESET
MS Code : PCMI-D-15-00027 | ☑ CP | ☑ DISK

for the isolation of pollutants and could be used as backfill in high-level nuclear waste repositories (Gates et al. 2009). Finally, smectites such as hectorite can form as secondary minerals during the alteration of nuclear glass containing high-level waste (Thien et al. 2010). These newly formed minerals can further react with hazardous radionuclides released by alteration of nuclear glass. Thus, it is important to understand the smectite crystallochemical properties which ultimately control their reactivity.

Smectites can exhibit a large variation in chemical compositions as a result of their versatile structure and of cationic substitution in crystal sites. For example, montmorillonite, the common aluminum smectite in soils and sediments, is made by the condensation of one octahedral sheet sandwiched between two tetrahedral sheets (Fig. 1), forming a TOT structure. Two-thirds of the octahedral sites are occupied mostly by Al(III), forming a dioctahedral framework in which Al(III) can be substituted by cations such as Mg(II) or Fe(II, III) (Stucki 1988). In contrast, in trioctahedral hectorite, all octahedral sites are filled, mostly by Mg(II), which can be substituted by Li(I) or trace amounts of Fe(II, III). Not only the extent, but also the distribution of chemical substitution can affect the chemical reactivity of smectite (Mering and Glaeser 1954). For example, reduction or oxidation of redox sensitive cations will modify the layer charge and thus alter properties such as swelling and/or cation-exchange capacity (Gates et al. 1996, 1998), which in turn may affect the retention capacities of bentonites.

Structural Fe in clay minerals can significantly impact the redox properties in the environments where they are present. The reduction of Fe(III) in smectite can be achieved by microbial (e.g., Pentráková et al. 2013) and by chemical treatments (e.g., Komadel et al. 2006; Stucki 2006). For example, ferruginous smectite can be reduced by dithionite within hours, and the reduction proceeds from the basal surfaces rather than from the particle edges (Komadel et al. 2006). Fe(II) in clay minerals is able to reduce heavy metals (Bishop et al. 2014) and radionuclides (Bishop et al. 2011; Yang et al. 2012), thereby modifying their mobility and availability. In contrast, Fe(III) may act as terminal electron acceptor for iron-reducing bacteria, which provides a mechanism of structural Fe(II) (re)generation (Ernstsen et al. 1998). The magnitude and reversibility of these reactions largely depend on the Fe local environment in the octahedral sheet, i.e., the formation of a solid solution or the occurrence of Fe-rich clusters (Drits and Manceau 2000) which can be controlled in part by the smectite structure. For example, in dioctahedral smectites, two octahedral sites of distinct sizes can be identified, and Fe(III) would preferentially enter the largest one (Tsipursky and Drits 1984), and thus be relatively dispersed. In contrast, preferential clustering of Fe was observed in trioctahedral micas, i.e., non-swelling phyllosilicates with TOT layers as in smectites (Manceau et al. 1990). This suggests that Fe distribution may differ depending on the octahedral sheet framework (dioctahedral or trioctahedral) of smectites. Unfortunately, no study reported unambiguous evidence for random Fe distribution in trioctahedral smectites so far.

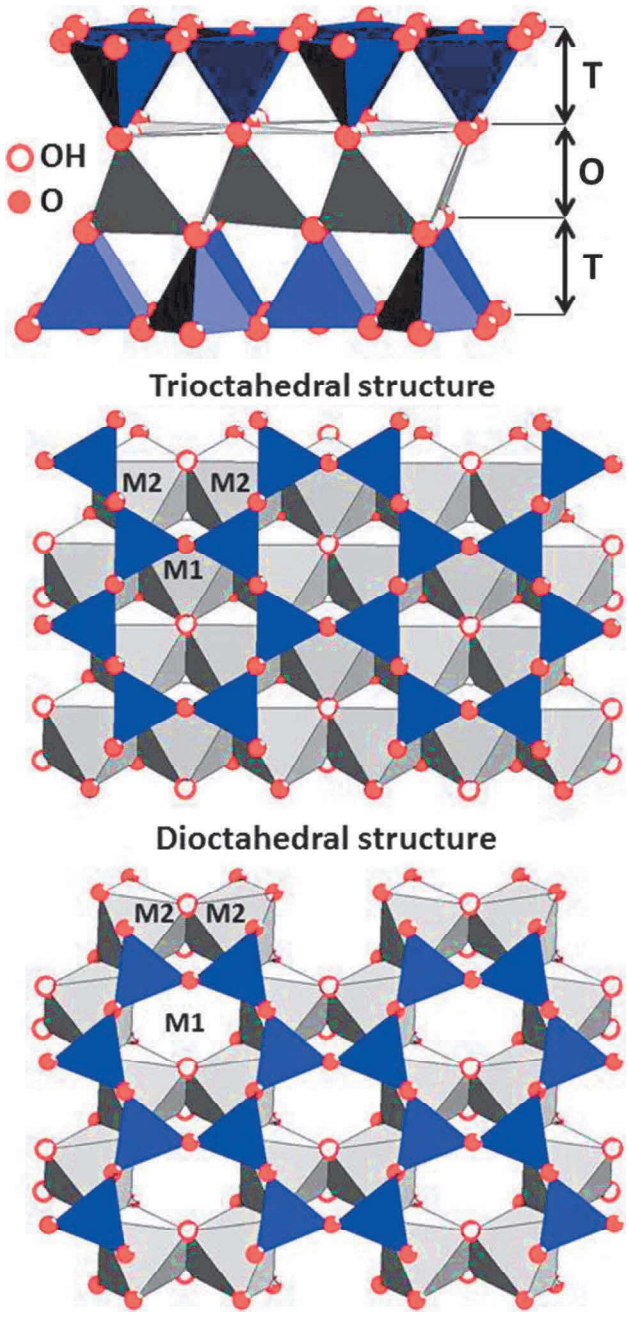

Fig. 1 *Top*: Structure of smectite. T: tetrahedral sheet, O: octahedral sheet. *Middle*: projection down *c** of trioctahedral framework. *Bottom*: projection down *c** of dioctahedral framework. *Blue triangles* are (Si, Al)O_4 tetrahedra; one tetrahedral sheet is not shown. M1 denotes *trans* sites, and M2 *cis* sites

Journal : Large 269 | Dispatch : 7-8-2015 | Pages : 13
Article No : 768 | LE | TYPESET
MS Code : PCMI-D-15-00027 | CP | DISK

X-ray absorption spectroscopy (XAS) and more specifically extended X-ray absorption fine structure (EXAFS) spectroscopy have proven to be reliable techniques to probe the molecular environment of transition metals. Powder EXAFS spectroscopy was used to investigate the Fe environment in montmorillonite (SWy-1) (Vantelon et al. 2003). No Fe–Fe pair was detected, suggesting that the structure has an ordered Fe distribution obeying an exclusion rule in the octahedral sheet. The spectroscopic analysis of such powder samples is, however, complicated by textural effects which are difficult to avoid during sample preparation of minerals having a layered structure (Manceau 1990). Powder EXAFS spectra for such anisotropic samples should be recorded with the sample plane oriented at the magic angle (at which any angular dependence is extinguished); otherwise, XAS analysis will provide an inaccurate description of the local environment. Unfortunately, information concerning sample preparation and orientation with respect to the incoming X-ray beam is most of the time missing. Additionally, EXAFS analysis for such samples is complicated by interferences between EXAFS waves scattered by neighboring shells located at similar distances from the absorber. This complication can be overcome by polarized EXAFS (P-EXAFS) spectroscopy which can discriminate the contributions of absorber–backscatterer pairs with distinct crystallographic orientations. This is of high interest in investigations on clay minerals where cationic shells from the tetrahedral and octahedral sheets are separated by <0.25 Å. The theoretical background and principle of P-EXAFS applied to smectite preparation are well documented (e.g., Manceau et al. 1998, 2000b; Schlegel et al. 1999). Thus, P-EXAFS can provide unique information on the nature, number, distance, and orientation of neighboring shells. For Fe, this information can be complemented by the analysis of pre-edge peaks which are related to quadrupolar and (forbidden) dipolar transitions from the 1*s* to *d* orbitals. The position and amplitude of these peaks are known to be sensitive to the oxidation state and the site symmetry of Fe (Manceau and Gates 1997; Wilke et al. 2001). The combination of pre-edge peaks and P-EXAFS spectroscopy was powerful in determining the Fe short-range environment in Fe-rich smectites such as nontronites (Gates et al. 2002; Manceau et al. 2000a, b).

In this study, the Fe chemical state and distribution in dioctahedral montmorillonite (SWy-1) and trioctahedral hectorite (SHCa-1) were investigated by XAS. These smectites are taken as representative of dioctahedral and trioctahedral clay minerals. In addition, these minerals are also model systems for material present in the backfill of a nuclear waste repository site and as a secondary phase frequently detected in alteration experiments of nuclear glass, respectively. As such, thorough determination of their crystallochemical properties is useful to improve the robustness of long-term models of waste confinement. In this study, oriented self-supporting films were prepared in order to probe the Fe *K*-edge by P-EXAFS spectroscopy for SWy-1 and, for the first time, SHCa-1. Also, P-XAS data were collected and analyzed to understand how Fe can affect the local structural properties of dioctahedral or trioctahedral smectites.

Experimental

Samples

Montmorillonite (SWy-1) and hectorite (SHCa-1) were purchased from the Source Clays Repository of the Source Clay Mineral Project (SCMP). Montmorillonite was purified according to a standard procedure described in (Golubev et al. 2006), and the fraction <1 μm was isolated. For hectorite, the fraction <2 μm was isolated by sedimentation and purified following the procedure described in (Schlegel et al. 1999). The purified montmorillonite and hectorite fractions were saturated with Na. The elemental compositions of the purified fractioned samples were determined by acid digestion and ICP-MS (Thermo X-Series II) analysis of the resulting solutions. The results are presented in Table 1. Besides the elements listed in Table 1, hectorite also contains large amounts of fluorine [2.7 % for the SCMP hectorite (Thomas et al. 1977)], but this element was not quantified because the analysis involved acid digestion using concentrated HF.

To remove possible X-ray amorphous ferric oxides during the purification, hectorite underwent a treatment with dithionite–citrate–bicarbonate that imposes strongly reducing conditions, followed by treatment with hydrogen peroxide that imposes strongly oxidizing conditions. With dithionite, a complete reduction of structural Fe from a trivalent to a divalent oxidation state can be achieved in

Table 1 Main cations content of montmorillonite (SWy-1) and hectorite (SHCa-1) determined by chemical analysis (other includes oxygen and fluorine)

(wt%)	Li	Mg	Al	Si	Fe	Other	Total
SWy-1	<0.01	1.36 (±0.01)	8.93 (±0.07)	25.84 (±3.30)	2.30 (±0.14)	61.57	100.00
SHCa-1	0.39 (0.01)	12.15 (±0.09)	0.40 (±0.01)	21.08 (±2.69)	0.24 (±0.01)	65.74	100.00

Journal : Large 269 | Dispatch : 7-8-2015 | Pages : 13
Article No : 768 | ☐ LE | ☐ TYPESET
MS Code : PCMI-D-15-00027 | ☑ CP | ☑ DISK

smectites, such as reported for the Fe-rich SWa-1 (Gorski et al. 2012) and for the montmorillonite SWy-2 (Neumann et al. 2011), and subsequent re-oxidation can be achieved with hydrogen peroxide (Gorski et al. 2013). Furthermore, reported spectroscopic data showed that structural changes in the Fe coordination environment and in the silicate lattice can be caused by the Fe reduction and that these are not fully reversible [e.g., SWy-2 and SWa-1, (Gorski et al. 2013; Neumann et al. 2011)]. Similarly to the reported montmorillonite data, Fe in hectorite may also have undergone a reduction–oxidation cycle, resulting in partly irreversible structural modifications. However, our infrared spectra do not reveal any strong perturbation of the hectorite lattice, certainly due to the low Fe content.

Purified Na-saturated smectites were first characterized by powder X-ray diffraction and Fourier-transform infrared (FTIR) spectroscopy. X-ray diffractograms were collected on oriented samples with a D8 Advance (Bruker) diffractometer (Cu K_α radiation) equipped with an energy-dispersive detector (Sol-X). FTIR spectra were obtained with a Bruker IFS 55 spectrometer, equipped with an attenuated total reflectance (ATR) cell and an mercury cadmium telluride (MCT) detector. Self-standing films were prepared by slow filtration of the clay suspensions on a 0.025-µm-pore-size filter (Millipore) (Schlegel et al. 1999). This protocol readily provided highly textured self-supporting films to perform polarized XAS experiments, with *a* and *b* layer axes of the crystallites randomly oriented in the plane of the film.

X-ray absorption spectroscopy (XAS)

Polarized Fe *K*-edge XAS data of the oriented clay samples were collected at the FAME beamline (Proux et al. 2005) at the ESRF (Grenoble, France) with a ring energy of 6 GeV and a ring current of 50–90 mA. The data were collected in fluorescence yield detection mode using a 30-element Ge solid-state detector (Canberra) at angles (α) between the electric field of the X-ray beam and the clay layer plane of 10°, 35°, 55° and 80°. The energy calibration was done by setting the first inflection point of the Fe *K*-edge of an iron foil at 7112.0 eV.

The pre-edge spectra were modeled by pseudo-Voigt line shapes (Westre et al. 1997) after subtraction of the baseline with an exponential function. The energy position, the full width at half maximum and the peak height were fit using a fixed 50:50 Gaussian/Lorentzian ratio for the peaks. The pre-peak intensity was calculated as the integrated areas of the pseudo-Voigt functions used for peak modeling.

Analysis of the EXAFS data was performed following standard procedures by using the Athena and Artemis interfaces to the IFEFFIT software (Ravel and Newville 2005). The spectra were extracted from the raw data, and the Fourier transforms (FTs) were obtained from the $k^3 \times \chi(k)$ functions (3.2–10.2 $Å^{-1}$ for both samples at all angles). The spectral data were fit in *R* space (1.3–3.8 Å for both samples at all angles) using phase and amplitude functions calculated with feff8.4 (Ankudinov et al. 1998). The amplitude reduction factor (S_0^2) was set to 0.70, a value well suited to properly fit the data of α-Fe (data not shown). In order to generate theoretical paths, the published structures of montmorillonite (Tsipursky and Drits 1984) and hectorite (Breu et al. 2003) were used with the absorber (Fe) located at octahedral position. Since the differences in backscattering amplitude between neighboring Mg, Al and Si are limited, the XAS fitting models were simplified. In montmorillonite, octahedral and tetrahedral contributions were fit by using only Al and Si backscatterers, respectively. In hectorite, only Mg (octahedral) and Si (tetrahedral) contributions were considered. Similarly, O and F only differ by Z ± 1 so that F neighbors in hectorite can be fitted with EXAFS phase and amplitude functions for O with only minimal discrepancy. Thus, the first coordination shell of Fe in hectorite can be considered to be made of O atoms only for fitting purposes.

For a given film, the data were fit simultaneously at all angles using a single value of ΔE, and for a given shell a common bond length and mean square displacement ("Debye–Waller" factor). The Fe/Al (montmorillonite) and Fe/Mg (hectorite) ratios were kept equal at all angles. The uncertainties are typically ±0.02 Å on the distances for well-resolved atomic shells and ±20 % on the coordination numbers. The experimental uncertainty on α is estimated to ±1°. The fit quality was quantified by the R_f factor representing the absolute misfit between theory and data (Ravel 2000).

Results and discussion

X-ray diffraction and infrared spectroscopy

X-ray diffractograms for the two smectites are presented in Fig. 2. The basal spacing for montmorillonite ($d(001)$ = 12.2(2) Å) and hectorite ($d(001)$ = 14.8(2) Å) is typical of smectite with one or two interlayer water molecules, respectively (Meunier 2005). Quartz (peak at 26.6°2θ) is also present in small quantities in montmorillonite, but could not be detected in hectorite. Quartz does not contain Fe and thus will not affect XAS measurements. No other crystalline phase could be detected, and the flat backgrounds of the diffractograms indicate the absence of additional X-ray amorphous phase.

The IR spectrum of montmorillonite (Fig. 2) matches reported data (Madejova and Komadel 2001), with an –OH stretching band of structural hydroxyl groups at 3623 cm^{-1}

Journal : Large 269 | Dispatch : 7-8-2015 | Pages : 13
Article No : 768 | ☐ LE | ☐ TYPESET
MS Code : PCMI-D-15-00027 | ☑ CP | ☑ DISK

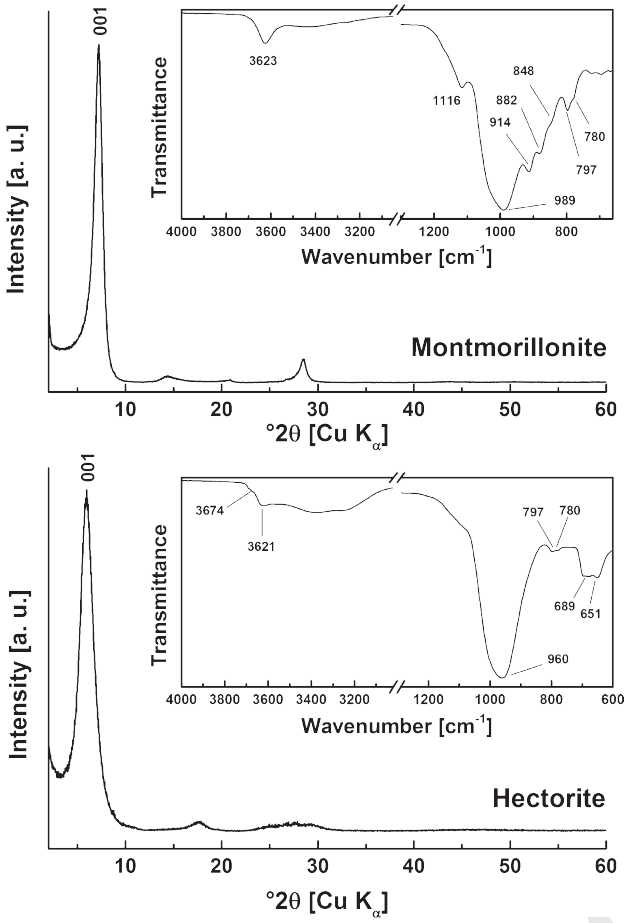

Fig. 2 X-ray diffractogram (basal spacing or *d*(001) is indexed) and ATR-FTIR spectrum of the clay fractions investigated in this study. *Top*: Montmorillonite. *Bottom*: Hectorite

and Si–O stretching bands at 989 and 1116 cm^{-1} (longitudinal mode). The spectrum also contains AlAl–OH, AlFe(III)–OH and AlMg–OH deformation bands at 914, 882 and 848 cm^{-1}, respectively. The spectrum of hectorite also matches reported data (Madejova and Komadel 2001), with –OH stretching bands of structural hydroxyl groups (3674 cm^{-1}) and bonded water (3621 cm^{-1}). The presence of adsorbed water is further indicated by two broad bands at 3380 cm^{-1} (–OH stretching) and ~3265 cm^{-1} (overtone of –OH deformation of water). This finding indicates that the interlayer of hectorite contains more water than that of montmorillonite for which these bands are absent, what is consistent with 2-layer and 1-layer hydrate state, respectively, determined by XRD. In hectorite, the bands at 960 and 689 cm^{-1} correspond to Si–O stretching and the band at 651 cm^{-1} to Mg_3–OH deformation. The trioctahedral character of this smectite is revealed by the Mg_3–OH band and the position of the structural hydroxyl group. The Si–O stretching bands at 780 and 797 cm^{-1} can be related to the presence of quartz in both samples (Madejova and Komadel 2001). The two bands are of similar intensity in hectorite, but not in montmorillonite, possibly because the band at 797 cm^{-1} in montmorillonite can also contain contribution from the Fe(III)Mg–OH bending mode (Gates 2008). No other phases could be detected.

The XRD and IR data indicate that the smectite preparations were free from Fe-containing ancillary phases, attesting to the success of the purification procedures. Also, –OH bands where the hydroxyl groups are connected to Fe octahedra were detected in the IR spectrum of montmorillonite, but not in hectorite, probably due to the low Fe content of this mineral. FeFe–OH deformation bands were absent in the two spectra, excluding Fe clustering and thus hinting at a random Fe distribution, at least in montmorillonite.

Pre-edge spectroscopy

The Fe *K*-edge XAS spectra have a weak pre-edge feature ~15 eV below the main absorption edge arising predominantly from the $1s \rightarrow 3d$ (quadrupolar) transition. However, the $1s \rightarrow 3d$ transition is electric dipole forbidden by parity considerations in a centrosymmetric octahedral environment (e.g., O_h symmetry) (Westre et al. 1997), but a very weak pre-edge feature, split into t_{2g}- and e_g-like components, is still experimentally observed, the intensity depending on the local symmetry and on the cation electronic properties. The pre-peak intensity can thus be used to evaluate the Fe oxidation state and coordination geometry (Manceau and Gates 1997; Manceau et al. 2000b; Wilke et al. 2001). For example, a higher pre-edge amplitude is observed for fourfold-coordinated Fe compared to sixfold-coordinated Fe, a consequence of mixing 3*d* and 4*p* atomic orbitals in T_d symmetry (Westre et al. 1997).

The pre-edge is located at around 7114.5 eV for both AQ1 montmorillonite and hectorite (Fig. 3), indicating that Fe is in an oxidation state of +III in both clays. The intensity of the pre-edges is weak (~1.5 % of the main edge), suggesting that Fe atoms are predominantly sixfold coordinated. The pre-edge features were modeled with pseudo-Voigt line shapes (Westre et al. 1997) to gain additional information on their amplitude and position (Fig. 4). At $\alpha = 35°$ (polarized and powder XAS data are identical at this angle), the difference in energy (Table 2) of the components for montmorillonite (1.49 eV) compared to hectorite (1.45 eV) is below the uncertainty associated with the position of the features (~0.1 eV). The total pre-peak intensities (i.e., total integrated areas, Table 2) equal 0.097 and 0.094 for montmorillonite and hectorite, respectively. These low values were compared with those obtained for sixfold-coordinated Fe(III) (Wilke et al. 2001). Also, the total pre-peak intensities are similar in both smectites. Interestingly, the ratio between the intensity of the contributions at lower to higher energies equals 1.31 for montmorillonite

Journal : Large 269 | Dispatch : 7-8-2015 | Pages : 13
Article No : 768 | LE | TYPESET
MS Code : PCMI-D-15-00027 | CP | DISK

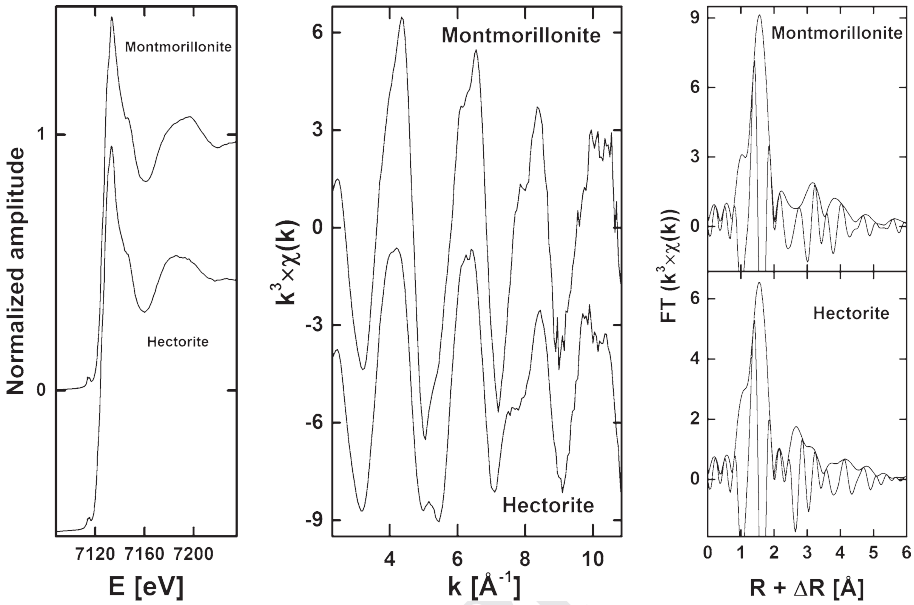

Fig. 3 Comparison of experimental Fe *K*-edge XANES (*left*), and EXAFS spectra (*middle*) recorded at $\alpha = 35°$ for montmorillonite and hectorite with the corresponding Fourier transforms (*right*)

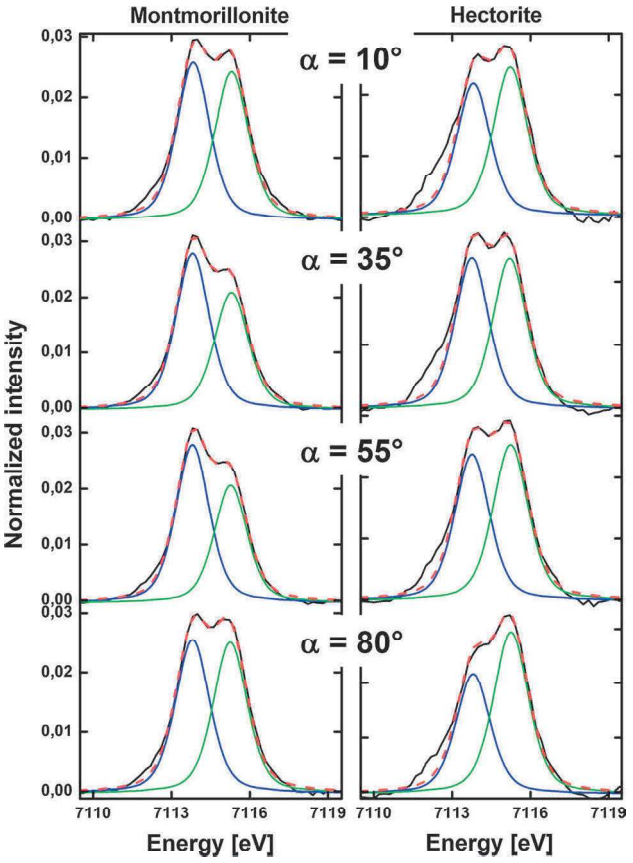

Fig. 4 Normalized pre-edge spectra (*solid black line*) and best fits (*dashed red lines*) with individual components (*blue* and *green thin lines*) for montmorillonite (*left*) and hectorite (*right*)

and 1.00 for hectorite. The intensity ratio of montmorillonite is close to expectation for octahedral high-spin ferric Fe (3:2) (Westre et al. 1997). The lower value for hectorite may best be explained by site distortion for Fe substituting for Mg/Li in the trioctahedral smectite. However, the low pre-peak intensity compared to the main edge suggested that the site is centrosymmetric and that such site distortion is actually limited. Alternatively, the observed difference may be explained by distinct covalence of the chemical bonds between Fe and the surrounding ligands (Westre et al. 1997). The e_g set of the 3*d* orbitals is more covalent than the t_{2g} set due to σ bonding with the ligands. Hectorite contains significant amount of fluorine substituting for OH groups, and because F has an electronegativity higher than O, the observed differences may also be attributed to Fe binding to F in hectorite. Regardless of the correct interpretation, these dissimilarities in pre-peak intensities indicate slight differences in Fe local environments.

The pre-peak intensity ratios do not exhibit a monotonic trend with α, consistent with previous observations on Fe-rich phyllosilicate (Dyar et al. 2001). For montmorillonite, the ratio increases from 10° to 55° and then decreases, whereas for hectorite it increases from 10° to 35° and then decreases. Since a dipole transition would be dichroic in nature, this complex angular behavior suggests that the transition is predominantly quadrupole (Hahn et al. 1982). The weakness of the dipole contribution corroborates the predominantly octahedral nature of the coordination polyhedra (Munoz et al. 2013).

Journal : Large 269 | Dispatch : 7-8-2015 | Pages : 13
Article No : 768 | ☐ LE | ☐ TYPESET
MS Code : PCMI-D-15-00027 | ☑ CP | ☑ DISK

Table 2 Results from the pre-edge fitting (uncertainties on the energies are estimated to 0.1 eV and 10 % on the intensities)

Sample	α	Pre-edge peak energy [eV]	Pre-edge peak intensity[a]	Peak energy difference[b]	Peak intensity ratio[c]
Montmorillonite	10°	7113.83	0.050	1.48	1.04
		7115.31	0.048		
	35°	7113.81	0.055	1.49	1.31
		7115.30	0.042		
	55°	7113.81	0.055	1.46	1.38
		7115.27	0.040		
	80°	7113.81	0.051	1.44	1.02
		7115.25	0.050		
Hectorite	10°	7113.82	0.042	1.41	0.88
		7115.23	0.048		
	35°	7113.76	0.047	1.45	1.00
		7115.21	0.047		
	55°	7113.77	0.048	1.47	0.92
		7115.24	0.052		
	80°	7113.81	0.044	1.45	0.72
		7115.26	0.061		

[a] Peak intensities correspond to integrated areas

[b] Peak energy differences correspond to energy differences between the lowest energy and the highest energy pre-edge features

[c] Ratio of the lowest energy peak intensity to the highest energy peak intensity

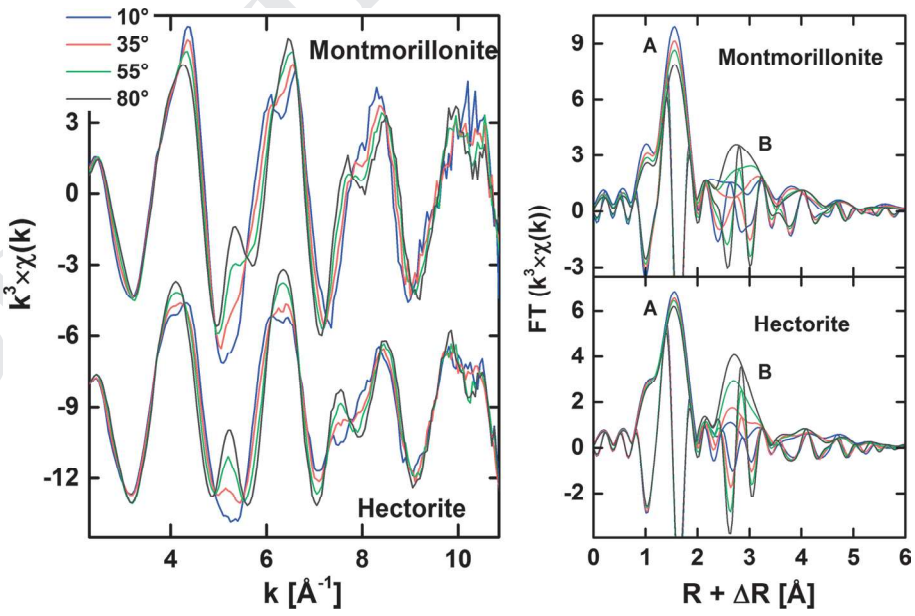

Fig. 5 Experimental P-EXAFS spectra (*left*) with the corresponding Fourier transforms (*right*) for montmorillonite and hectorite

EXAFS spectroscopy

EXAFS spectra

Both sets of P-EXAFS spectra exhibit a significant angular dependence over the whole k range, and well-defined isosbestic points are observed, attesting to the high degree of particle orientations in the self-supporting films (Fig. 5). The variation in amplitude and position of the maxima at ~4.2, 5.3, 6.5, 8.0 and 9.1 $Å^{-1}$ is consistent with the presence of atomic shells with distinct orientations, e.g., in-plane Mg/Al/Fe and out-of-plane Si atoms. The large dependence on polarization is also consistent with the successful preparation of highly oriented clay films.

Journal : Large 269 | Dispatch : 7-8-2015 | Pages : 13
Article No : 768 | LE | TYPESET
MS Code : PCMI-D-15-00027 | CP | DISK

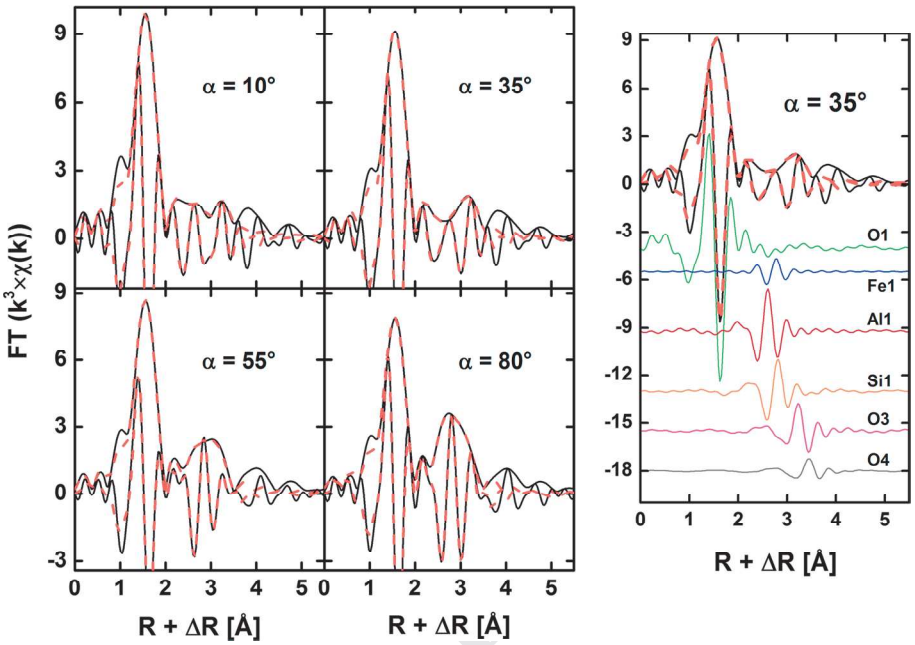

Fig. 6 Experimental (*solid black lines*) and modeled (*dashed red lines*) polarized Fourier transforms for the montmorillonite data. The *right panel* indicates the contributions at $\alpha = 35°$ of the single atomic shells

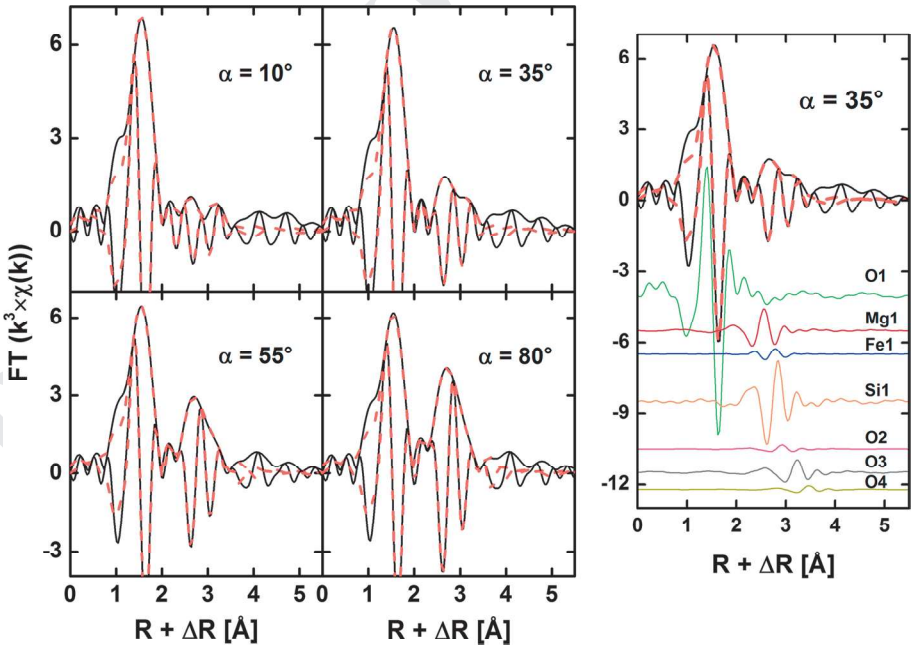

Fig. 7 Experimental (*solid black lines*) and modeled (*dashed red lines*) polarized Fourier transforms for the hectorite data. The *right panel* indicates the contributions at $\alpha = 35°$ of the single atomic shells

The powder EXAFS spectra recorded at $\alpha = 35°$ for montmorillonite and hectorite show subtle differences in the position and amplitude of oscillation maxima, e.g., at $k \sim 5.0$, 6.3 and 8.0 Å^{-1} (Fig. 3). The presence of distinct frequencies suggests that Fe has distinct molecular environments in terms of nature and number of backscattering atoms, consistent with the dioctahedral nature of montmorillonite and the trioctahedral nature of hectorite. This is also clearly seen on the corresponding Fourier transforms (FT) where the contributions from the cationic shells differ.

Fourier transforms

The FTs contain several peaks (Fig. 5). Peak A ($R + \Delta R \sim 1.6$ Å) corresponds to the first oxygen shell (O1), and its magnitude is higher in montmorillonite than in hectorite. Best fits (Figs. 6 and 7) were obtained for Fe–O1 interatomic distances of $R_{\text{Fe-O1}} = 2.01(1)$ Å in montmorillonite and 2.00(1) Å in hectorite (Tables 3 and 4). These bond lengths are characteristic of sixfold-coordinated Fe(III) and match reported values for Fe located at clay octahedral sites (Manceau et al. 1998, 2000b; Vantelon

Journal : Large 269 | Dispatch : 7-8-2015 | Pages : 13
Article No : 768 | LE | TYPESET
MS Code : PCMI-D-15-00027 | CP | DISK

Table 3 Quantitative EXAFS analysis for montmorillonite

α	Fe ↔ O1			Fe ↔ Fe1			Fe ↔ Al1		
	N	R [Å]	σ^2 [Å^2]	N	R [Å]	σ^2 [Å^2]	N	R [Å]	σ^2 [Å^2]
10°	6.3(5)	2.01(1)	0.005	0.5(1)	3.02(1)	0.004	3.4(3)	3.04(1)	0.004
35°	5.8(5)			0.4(1)			2.6(3)		
55°	5.5(5)			0.2(1)			1.4(5)		
80°	4.9(4)			0.1(1)			0.6(1)		

α	Fe ↔ Si1			Fe ↔ O3			Fe ↔ O4			ΔE_0 [eV][a]	R_f ($\times 10^3$)[b]
	N	R [Å]	σ^2 [Å^2]	N	R [Å]	σ^2 [Å^2]	N	R [Å]	σ^2 [Å^2]		
10°	1.4(7)	3.22(1)	0.007	5.4(1.6)	3.79(1)	0.004	2.4(2.4)	4.01(2)	0.007	6.8(4)	5.6
35°	3.4(3)			5.8(1.3)			4.2(1.9)				5.4
55°	5.2(5)			6.0(1.1)			6.3(1.6)				5.6
80°	6.6(7)			6.1(9)			8.0(1.3)				8.3

The data were fit over the entire range considering the data from both tables: N is the coordination number, R is the interatomic distance, σ^2 is the mean squared displacement. The number in parentheses indicates the uncertainty

[a] Shift in ionization energy, threshold energy E_0 taken as zero-crossing of the second derivative

[b] Figure of merit of the fit (Ravel 2000)

Table 4 Quantitative EXAFS analysis for hectorite

α	Fe ↔ O1			Fe ↔ Mg1			Fe ↔ Fe1			Fe ↔ Si1		
	N	R [Å]	σ^2 [Å^2]	N	R [Å]	σ^2 [Å^2]	N	R [Å]	σ^2 [Å^2]	N	R [Å]	σ^2 [Å^2]
10°	5.4(5)	2.00(1)	0.006	2.8(2)	3.03(1)	0.008	0.3(1)	3.03(3)	0.008	2.1(2)	3.24(1)	0.007
35°	5.1(5)			1.7(6)			0.2(1)			3.4(6)		
55°	4.9(4)			1.1(6)			0.1(1)			5.1(6)		
80°	4.6(4)			0.6(1)			0.1(1)			6.9(7)		

α	Fe ↔ O2			Fe ↔ O3			Fe ↔ O4			ΔE_0 [eV][a]	R_f ($\times 10^3$)[b]
	N	R [Å]	σ^2 [Å^2]	N	R [Å]	σ^2 [Å^2]	N	R [Å]	σ^2 [Å^2]		
10°	0.1(1)	3.48(1)	0.006	2.4(1.3)	3.78(1)	0.008	0.1(1)	4.01(1)	0.008	6.6(2)	4.7
35°	0.6(1.1)			2.8(1.5)			1.0(1.3)				3.6
55°	1.4(1.1)			3.9(1.6)			3.7(1.4)				2.9
80°	1.4(6)			4.1(1.9)			5.5(5)				4.4

The data were fit over the entire range considering the data from both tables: N is the coordination number, R is the interatomic distance, σ^2 is the mean squared displacement. The number in parentheses indicates the uncertainty

[a] Shift in ionization energy, threshold energy E_0 taken as zero-crossing of the second derivative

[b] Figure of merit of the fit (Ravel 2000)

et al. 2003). The greater amplitude of peak A for montmorillonite correlates with a greater number of detected O1 neighbors, e.g., at α = 35°, N_{O1} = 5.8(5) for montmorillonite and 5.1(5) for hectorite (Tables 3 and 4). The slightly lower N_{O1} in hectorite can be related to a larger structural disorder resulting in a broader distribution of Fe–(O, F) bond lengths (Manceau et al. 2000b) around a mean value, which is consistent with the pre-edge results.

The amplitude of peak A decreases for both smectites, and the decrease is more pronounced in montmorillonite than in hectorite (Fig. 5). Fits (Figs. 6 and 7) indicate that N_{O1} decreases from 6.3(5) at $\alpha = 10°$ to 4.9(4) at $\alpha = 80°$ for montmorillonite and from 5.4(5) to 4.6(4) for hectorite (Tables 3 and 4). Using the relationship between N as a function of α and the angle β between the X-ray absorber–backscatterer pair and the normal to the film plane (Schlegel et al. 1999), the orientation of the O1 shell can be estimated. The calculated values of β_{O1} equal 58.1(1.5)° and 56.9(7)° for montmorillonite and hectorite, respectively. Though the value obtained for montmorillonite deviates significantly from the value expected for fully symmetric octahedra (54.7°), they are consistent with the

Journal : Large 269 | Dispatch : 7-8-2015 | Pages : 13
Article No : 768 | LE | TYPESET
MS Code : PCMI-D-15-00027 | CP | DISK

octahedral flattening observed in most hydrous TOT phyllosilicates (Güven 1988).

Peak B ($R + \Delta R$ ~ 2.75 Å) corresponds to the sum of contributions from the nearest octahedral (Mg, Al, Fe) shell (montmorillonite) or (Mg, Li) shell (hectorite), the nearest tetrahedral Si shell and the next nearest O shell. The position, amplitude and angular dependences of this peak depend on the interferences between the EXAFS contributions from the octahedral and tetrahedral sheets. For example, peak B for montmorillonite displays a complex polarization dependence: Its amplitude decreases from $\alpha = 10°$ to $\alpha = 35°$ and then increases with α, and the position and imaginary parts shift to higher $R + \Delta R$ values with α (Fig. 5). In smectites, this angular behavior is diagnostic of in-plane predominant contributions from (Mg, Al) cations in the octahedral sheet, and out-of-plane contributions from tetrahedral Si (Schlegel et al. 1999). This peak was fit assuming Fe, Al and Si contributions at $R_{\text{Fe-Fe1}} = 3.02(1)$ Å, $R_{\text{Fe-Al1}} = 3.04(1)$ Å and $R_{\text{Fe-Si1}} = 3.22(1)$ Å, respectively (Table 3). Best-fit bond distances match values obtained from diffraction data (Tsipursky and Drits 1984). For increasing α values, the coordination numbers decrease from 0.5(1) to 0.1(1) for the Fe shell, from 3.4(3) to 0.6(1) for the Al shell, and increase from 1.4(7) to 6.6(7) for the Si shell (Table 3). These angular dependences are consistent with Al and Fe shells oriented predominantly in the in-plane dimension, while the Si shell is oriented in the out-of-plane direction. The numbers of neighboring atoms obtained at $\alpha = 35°$ ($N_{\text{Fe1}} = 0.4(1)$, $N_{\text{Al1}} = 2.6(3)$ and $N_{\text{Si1}} = 3.4(3)$) are in reasonable agreement with coordination numbers for montmorillonite [three (Al, Fe) neighbors in-plane and four (Si, Al) neighbors out-of-plane]. The fit results indicate a small but significant contribution from neighboring Fe and thus the presence of Fe–Fe pairs. This finding is based on the ability of P-EXAFS to filter out overlapping contributions from shells with distinct orientations, thereby decreasing uncertainties on structural parameters. This can explain, at least partly, why our results slightly differ from earlier conclusions based on the analysis of powder EXAFS spectra (Vantelon et al. 2003).

In contrast to montmorillonite, the amplitude of peak B in hectorite increases with α and its position varies only slightly (Fig. 5). Peak B was modeled considering Mg, Fe and Si shells at $R_{\text{Fe-Mg1}} = 3.03(1)$ Å, $R_{\text{Fe-Fe1}} = 3.03(3)$ Å and $R_{\text{Fe-Si1}} = 3.24(1)$ Å, respectively (Table 4). The bond distances are consistent with values obtained from diffraction data for Mg and Si shells (Breu et al. 2003), and $R_{\text{Fe-Fe1}}$ is typical of edge-sharing Fe octahedra. The coordination numbers of octahedral Mg and Fe decrease from 2.8(2) to 0.6(1) and from 0.3(1) to 0.1(1), respectively, and increase for Si from 2.1(2) to 6.9(7), for increasing α values (Table 4). The angular dependences are consistent with Mg and Fe shells located in-plane and Si located out-of-plane, but the in-plane number of neighboring Mg + Fe is much lower than expected from the smectite composition. For a trioctahedral structure, six octahedral and four tetrahedral cationic neighbors would be expected. The detected number of tetrahedral neighbors equals 3.4(6), reasonably close to the theoretical value of four, but the number of octahedral neighbors equals ~2, much lower than the expected value of six (Table 4). Several explanations could possibly explain the deviation from the ideal values. First, hectorite contains Li substituting for Mg (Table 1), and Li is too light to be detected by EXAFS spectroscopy. The impact of this substitution on N_{Mg} can be estimated from the Li/Mg ratio of ~1:10 in hectorite. Assuming random distributions of Mg and Li in the octahedral sheet, the detected number of Mg neighbors should be close to 5.4, a value still significantly higher than the experimental value. Second, as Fe(III) substitutes for Mg(II), the increase in local charge may be balanced by vacancies or more likely by Li(I) preferential insertion in adjacent octahedral sites, thereby lowering the number of detected octahedral neighbors. A third hypothesis is that electronic waves backscattered by octahedral Fe and Mg/Al are out of phase (Manceau 1990) leading to destructive interferences as can be seen in Figs. 6 and 7. Owing to this interference, the apparent numbers of Fe and Mg neighbors are mutually lowered and so actual number of neighboring Fe (and Mg) cations. Please note that such interference would also occur in powder spectra, and would be further compounded by the EXAFS contribution of out-of-plane Si. Peak B for hectorite also contains contribution from the next nearest oxygen shell [$N_{\text{O2}} = 0.6(1.1)$] located on the basal plane ($R_{\text{Fe-O2}} = 3.48(1)$ Å). This shell is not detected in the dioctahedral smectite because of corrugation of the basal oxygen planes that increases the average spread of the Fe–O2 distances (Manceau et al. 2000a). From the increase in N_{O2} with α (Table 4), this shell is clearly located out-of-plane, matching expectation for a shell located at the basal plane.

Two additional O shells were also used to improve the fit of peak B at higher distances in both smectites (Tables 3 and 4). The O3 shell originates from O atoms of adjacent octahedra ($R_{\text{Fe-O3}} = 3.78$–3.79 Å) and the O4 shell from atoms of the basal planes of the silicate sheet ($R_{\text{Fe-O4}} = 4.01(1)$ Å), and the bond distances are close to reported values (Breu et al. 2003; Tsipursky and Drits 1984). For montmorillonite, the number of detected backscatterers at $\alpha = 35°$ [$N_{\text{O3}} = 5.8(1.3)$ and $N_{\text{O4}} = 4.2(1.9)$] match coordination numbers expected for smectites ($N_{\text{O3}} = 6$ and $N_{\text{O4}} = 4$), whereas they are much lower than expected for hectorite [$N_{\text{O3}} = 2.8(1.5)$ and $N_{\text{O4}} = 1.0(1.3)$]. This again suggests that the phyllosilicate local structure around Fe(III) is distorted in hectorite.

For montmorillonite and hectorite, N_{O4} increases from 2.4(2.4) to 8.0(1.3) and from 0.1(1) to 5.5(5), respectively,

Journal : Large 269 | Dispatch : 7-8-2015 | Pages : 13
Article No : 768 | LE | TYPESET
MS Code : PCMI-D-15-00027 | CP | DISK

for α increasing from 10° to 80°. These variations match expectations for the O4 shell located at the smectite basal planes, i.e., in out-of-plane direction. The O3 coordination number is invariant within uncertainty for both montmorillonite (N_{O3} = 5.4(1.6) to 6.1(9) for α = 10°–80°, respectively) and hectorite (N_{O3} = 2.4(1.3)–4.1(1.9) for α = 10°–80°, respectively). Thus, no clear angular dependence can be obtained from these values but they are compatible with the known orientation of the O3 shell inclined toward the octahedral sheet (Schlegel et al. 2001).

Discussion

X-ray diffraction and infrared data showed that both purified smectites are free from Fe-containing impurities, implying that Fe can only be located in the smectite structure. Infrared data are also consistent with a dioctahedral structure for montmorillonite and a trioctahedral structure for hectorite. The pre-edge and EXAFS spectroscopic data indicate that Fe is in trivalent oxidation state and located in the octahedral sheet but that the Fe local environments in the two clays are dissimilar. The bond lengths and the angular dependences of the neighboring atomic shells confirm this structural assignment and indicate that the amount of Fe in the tetrahedral sheet is marginal.

In montmorillonite, the number of cationic neighbors detected in-plane ($N_{Fe1} + N_{Al1} = 3$) is in agreement with a dioctahedral structure ($N = 3$). Fits to the data are consistent with Fe substituting for Al/Mg in the octahedral layer. Fe–Fe pairs were detected, but with a low number of backscatterers [$N_{Fe1} = 0.4(1)$]. The elemental composition (Table 1) indicates a moderate Fe content (2.3 wt%) and the corresponding (Al + Mg)/Fe molar ratio equals 9.4. Considering a fully random Fe distribution with all Al located in the octahedral sheet, about 0.3 neighboring Fe atom would be expected. This calculated value is similar to the fit results within uncertainties. This finding excludes Fe clustering and suggests that Fe is randomly distributed in montmorillonite. Earlier powder EXAFS analysis (Vantelon et al. 2003) also indicated an ordered Fe distribution in this montmorillonite but obeying an exclusion rule. However, powder XAS applied to sheet silicates is affected by larger uncertainties due to the interferences between waves backscattered by shells located at similar distances (Manceau 1990). This limitation was overcome in the present study by using the improved sensitivity of P-EXAFS spectroscopy, and low number of Fe backscatterers could be unambiguously detected. This improved sensitivity of P-EXAFS spectroscopy was subsequently applied to investigate in detail and for the first time, the Fe distribution in the trioctahedral hectorite.

In hectorite, all octahedral sites are filled by various cations such as Li, Mg, Al and Fe, and in addition some F substitutes for OH groups. This complex chemical composition of the octahedral sheet could somewhat complicate the powder EXAFS investigation of the Fe environment, thus requiring the use of P-EXAFS spectroscopy. The pre-edge is particularly sensitive to the electronic and geometric structure of the Fe site. The analysis of the hectorite pre-edge suggests differences in the binding environment compared to montmorillonite that may be attributed to some F substitution for OH groups. This substitution possibly distorted the site geometry and/or modified the ligand field. Although OH and F have similar ionic radii [r(OH) = 1.32 Å, r(F) = 1.29 Å in II-coordination (Shannon 1976)], F is more electronegative than O, which can decrease the length of the Fe–F bond compared to the Fe–O one. This is confirmed by reported $R_{Mg\text{-}O}$ and $R_{Mg\text{-}F}$ distances in hectorite (Breu et al. 2003) differing by ~0.06 Å. The Fe–(O, F)$_6$ coordination octahedron is thus probably slightly distorted, as corroborated by the slightly larger mean square displacement of the O1 shell in hectorite (σ^2 = 0.006 Å^2) compared to montmorillonite (σ^2 = 0.005 Å^2). The distribution of interatomic distances around a mean value dampens the EXAFS oscillatory contribution from the (O, F)1 shell, thus leading to a slightly lower number of neighboring (O, F) atoms. Furthermore, the mean square displacement is also larger for octahedral neighbors in hectorite (Mg, Fe) compared to montmorillonite (Al, Fe). However, previous NMR data have demonstrated Fe–F avoidance in phyllosilicate, i.e., F is usually not associated with Fe octahedra (Sanz and Stone 1983). Also, NMR investigation on hectorite failed to report evidence for Fe–F association, although this could be due to the minute amount of structural Fe (0.2 wt%) compared to the high F content (up to 5.18 wt% in some preparations) (Thomas et al. 1977). In addition, any distortion due to the presence of F is unlikely to result in a large incoherency of the distances between Fe and the neighboring cations. Indeed, the limited nature of this disorder is attested by the ability of conventional diffraction methods to derive a structural model for hectorite without the need of complex corrections (Breu et al. 2003; Oberlin and Mering 1966). The benign nature of this distortion is corroborated by the detection of similar numbers of Si atoms at very similar distances and comparable mean square displacement in both smectites.

Hectorite has a low Fe content (0.2 wt%), and the corresponding (Al + Mg)/Fe molar ratio equals 130. Considering a fully random distribution of Fe in the octahedral sheet, the number of neighboring Fe detected by EXAFS would be about 0.06, slightly smaller than the detected value of 0.2(1), values close to the lower limit of detection of EXAFS. This would suggest that Fe atoms within the octahedral sheet may preferentially form some pairs, as reported for trioctahedral micas (Manceau et al. 1990).

Journal : Large 269 | Dispatch : 7-8-2015 | Pages : 13
Article No : 768 | LE | TYPESET
MS Code : PCMI-D-15-00027 | CP | DISK

However, the extended formation of Fe(III) clusters within the octahedral sheet is ruled out because it would have led to much greater N_{Fe} values.

Fe is also surrounded by Mg neighbors, but the number of detected Mg is much smaller than the theoretical number for random distribution in hectorite ($N_{Mg} = 5.4$), which cannot be explained by structural disorder alone. In hectorite, almost all octahedral sites are filled with cations of similar sizes when sixfold coordinated by oxygen atoms [r^{VI}(Mg(II)) = 0.72 Å and r^{VI}(Li(I)) = 0.76 Å (Shannon 1976)], but of different charge. The sixfold-coordinated Fe(III) is slightly smaller (r^{VI}(Fe(III) = 0.65 Å) than Mg or Li so that the substitution would not result in significant lattice strain. However, Fe(III) insertion in octahedral sites may be locally charge-balanced by octahedral vacancies and/or by Li(I) filling neighboring octahedra. Because Li cannot be detected by EXAFS spectroscopy, these two hypotheses cannot be discriminated, but both of them would result in a low number of detected octahedral neighbors. In fact, the presence of vacancies surrounding Fe(III) would correspond to the local formation of a dioctahedral-like environment around Fe(III), a little similar to the Fe(III) local environment in montmorillonite. However, it would probably lead to a large deficit of local charge. Interestingly, in dioctahedral smectites, deficit of local charge can be decreased by thermal diffusion of Li(I) cations in vacant octahedra (Komadel et al. 2005). In the case of hectorite, such a diffusion would not be driven by heat, though, but would readily occur during crystallization. Other charge-balance mechanisms include the deprotonation of hydroxyl groups of the octahedral sheet close to Fe(III), but this would probably lead to severe distortion of the Fe coordination sphere. Still another mechanism of local charge compensation would be the substitution of Si(IV) by Al(III) in the tetrahedral sheet. From our EXAFS results, however, we surmise that local charge compensation is achieved by Li.

Conclusions

The local chemical environment around Fe in the dioctahedral smectite montmorillonite and, for the first time, in the trioctahedral smectite hectorite, was characterized by P-EXAFS spectroscopy. Iron(III) in these smectites is surrounded by in-plane (Mg, Al, Fe) atoms and out-of-plane Si atoms at distances in agreement with previous studies. Furthermore, Fe–Fe pairs in limited number could be unambiguously detected, owing to the ability of P-EXAFS to filter out overlapping contributions from shells with distinct orientations. Low numbers of neighboring Fe were detected, and no extended clustering could be observed in either of the minerals, indicating a next-to-random distribution of Fe in the octahedral sheet. Furthermore, the XAS data indicate that the substitution of Fe for Al in the dioctahedral montmorillonite does only marginally affect the local site symmetry. In contrast, the substitution of Mg(II) by Fe(III) in hectorite creates an excess of charge, which is balanced by a deficit of charge in the neighboring octahedra, either in the form of vacancies or as Mg(II) substitutions by Li(I). If confirmed, this result would provide a nice example on how impurities in clay minerals can drive heterogeneities in the charge distributions at clay mineral surfaces. The additional amount of lattice flexibility offered by the presence of vacant sites would also explain the ability of hectorite to incorporate large cations such as lanthanides (Finck et al. 2009) or actinides (Finck et al. 2015).

Acknowledgments The European Synchrotron Radiation Facility is acknowledged for provision of synchrotron radiation beamtime. We thank O. Proux for assistance during XAS data collection at the FAME beamline.

References

Ankudinov AL, Ravel B, Rehr JJ, Conradson SD (1998) Real-space multiple-scattering calculation and interpretation of X-ray-absorption near-edge structure. Phys Rev B 58(12):7565–7576

Bishop ME, Dong H, Kukkadapu RK, Liu C, Edelmann RE (2011) Bioreduction of Fe-bearing clay minerals and their reactivity toward pertechnetate (Tc-99). Geochim Cosmochim Acta 75(18):5229–5246

Bishop ME, Glasser P, Dong H, Arey B, Kovarik L (2014) Reduction and immobilization of hexavalent chromium by microbially reduced Fe-bearing clay minerals. Geochim Cosmochim Acta 133:186–203

Breu J, Seidl W, Stoll A (2003) Fehlordnung bei Smectiten in Abhängigkeit vom Zwischenschichtkation. Zeitschrift für anorganische und allgemeine Chemie 629(3):503–515

Drits VA, Manceau A (2000) A model for the mechanism of Fe3+ to Fe2+ reduction in dioctahedral smectites. Clays Clay Miner 48(2):185–195

Dyar MD, Delaney JS, Sutton SR (2001) Fe XANES spectra of iron-rich micas. Eur J Miner 13(6):1079–1098

Ernstsen V, Gates WP, Stucki JW (1998) Microbial reduction of structural iron in clays—a renewable source of reduction capacity. J Environ Qual 27(4):761–766

Finck N, Schlegel ML, Bosbach D (2009) Sites of Lu(III) sorbed to and coprecipitated with hectorite. Environ Sci Technol 43(23):8807–8812

Finck N, Dardenne K, Geckeis H (2015) Am(III) coprecipitation with and adsorption on the smectite hectorite. Chem Geol 409:12–19

Gates WP (2008) Cation mass-valence sum (CM-VS) approach to assigning OH-bending bands in dioctahedral smectites. Clays Clay Miner 56(1):10–22

Gates WP, Stucki JW, Kirkpatrick RO (1996) Structural properties of reduced upton montmorillonite. Phys Chem Miner 23:535–541

Gates WP et al (1998) Swelling and texture of iron-bearing smectites reduced by bacteria. Clays Clay Miner 46(5):487–497

Gates WP, Slade PG, Manceau A, Lanson B (2002) Site occupancies by iron in nontronites. Clays Clay Miner 50(2):223–239

Gates WP, Bouazza A, Churchman GJ (2009) Bentonite clay keeps pollutants at bay. Elements 5:105–110

Journal : Large 269 | Dispatch : 7-8-2015 | Pages : 13
Article No : 768 | ☐ LE | ☐ TYPESET
MS Code : PCMI-D-15-00027 | ☑ CP | ☑ DISK

Golubev SV, Bauer A, Pokrovsky OS (2006) Effect of pH and organic ligands on the kinetics of smectite dissolution at 25 °C. Geochim Cosmochim Acta 70(17):4436–4451

Gorski CA, Klüpfel LE, Voegelin A, Sander M, Hofstetter TB (2013) Redox Properties of structural Fe in clay minerals: 3. relationships between smectite redox and structural properties. Environ Sci Technol 47(23):13477–13485

Güven N (1988) Smectites. In: Bailey SW (ed) Hydrous phyllosilicates. Reviews in mineralogy. Mineralogical Society of America, Washington, DC, pp 497–559

Güven N (2009) Bentonites—clay for molecular engineering. Elements 5(2):89–92

Hahn JE et al (1982) Observation of an electric quadrupole transition in the X-ray absorption spectrum of a Cu(II) complex. Chem Phys Lett 88(6):595–598

Komadel P, Madejova J, Bujdak J (2005) Preparation and properties of reduced-charge smectites—a review. Clays Clay Miner 53(4):313–334

Komadel P, Madejová J, Stucki JW (2006) Structural Fe(III) reduction in smectites. Appl Clay Sci 34(1–4):88–94

Madejova J, Komadel P (2001) Baseline studies of the clay minerals society source clays: infrared methods. Clays Clay Miner 49(5):410–432

Manceau A (1990) Distribution of cations among the octahedra of phyllosilicates—insights from EXAFS. Can Miner 28:321–328

Manceau A, Gates WP (1997) Surface structural model for ferrihydrite. Clays Clay Miner 43:448–460

Manceau A, Bonnin D, Stone WEE, Sanz J (1990) Distribution of Fe in the octahedral sheet of trioctahedral micas by polarized EXAFS. Phys Chem Miner 17(4):363–370

Manceau A, Chateigner D, Gates WP (1998) Polarized EXAFS, distance-valence least-squares modeling (DVLS) and quantitative texture analysis approaches to the structural refinement of Garfield nontronite. Phys Chem Miner 25(5):347–365

Manceau A et al (2000a) Oxidation–reduction mechanism of iron in dioctahedral smectites: II. Crystal chemistry of reduced Garfield nontronite. Am Miner 85(1):153–172

Manceau A et al (2000b) Oxidation–reduction mechanism of iron in dioctahedral smectites: I. Crystal chemistry of oxidized reference nontronites. Am Miner 85(1):133–152

Mering J, Glaeser R (1954) Sur le rôle de la valence des cations échangeables dans la montmorillonite. Bulletin de la Société française de Minéralogie et Cristallographie 77:519–530

Meunier A (2005) Clays. Springer, Berlin Heidelberg

Munoz M et al (2013) Iron oxidation state in phyllosilicate single crystals using Fe-K pre-edge and XANES spectroscopy: effects of the linear polarization of the synchrotron X-ray beam. Am Miner 98(7):1187–1197

Neumann A, Petit S, Hofstetter TB (2011) Evaluation of redox-active iron sites in smectites using middle and near infrared spectroscopy. Geochim Cosmochim Acta 75(9):2336–2355

Oberlin A, Mering J (1966) Observations sur l'hectorite (étude en microscopie et diffraction électronique). Bulletin de la Société française de Minéralogie et Cristallographie 89:29–40

Pentráková L, Su K, Pentrák M, Stucki JW (2013) A review of microbial redox interactions with structural Fe in clay minerals. Clay Miner 48(3):543–560

Proux O et al (2005) FAME: a new beamline for X-ray absorption investigation of very-diluted systems of environmental materials and biological interest. Phys Scr T115:970–973

Ravel B (2000) EXAFS analysis with feff and feffit. Part 2. Commentary, New york

Ravel B, Newville M (2005) ATHENA, ARTEMIS, HEPHAESTUS: data analysis for X-ray absorption spectroscopy using IFEFFIT. J Synchrotron Radiat 12(4):537–541

Sanz J, Stone WEE (1983) NMR applied to minerals: 4. Local order in the octahedral sheet of micas: Fe-F avoidance. Clay Miner 18(2):187–192

Schlegel ML, Manceau A, Chateigner D, Charlet L (1999) Sorption of metal ions on clay minerals. I. Polarized EXAFS evidence for the adsorption of cobalt on the edges of hectorite particles. J Colloid Interface Sci 215:140–158

Schlegel ML, Manceau A, Hazemann J-L, Charlet L (2001) Adsorption mechanisms of Zn on hectorite as a function of time, pH, and ionic strength. Am J Sci 301(9):798–830

Shannon RD (1976) Revised effective ionic radii and systematic studies of interatomic distances in halides and chalcogenides. Acta Crystallogr Sect A 32(5):751–767

Stucki JW (1988) Structural iron in smectites. In: Stucki JW, Goodman BA, Schwertmann U (eds) Iron in soils and clay minerals. NATO ASI series. Springer, New york, pp 625–675

Stucki JW (2006) Chapter 8: properties and behaviour of iron in clay minerals. In: Bergaya F, Theng BKG, Gerhard L (eds) Developments in clay science. Elsevier, Buffalo Grove, pp 423–475

Swarnakar R, Brandt KB, Kydd RA (1996) Catalytic activity of Ti- and Al-pillared montmorillonite and beidellite for cumene cracking and hydrocracking [A3411]. Appl catal A Gen 142:161

Thien B et al (2010) Structural identification of a trioctahedral smectite formed by the aqueous alteration of a nuclear glass. Appl Clay Sci 49(3):135–141

Thomas J, Glass HD, White WA, Trandel RM (1977) Fluoride content of clay minerals and argillaceous earth materials. Clays Clay Miner 25(4):278–284

Tsipursky SI, Drits VA (1984) The distribution of octahedral cations in the 2-1 layers of dioctahedral smectites studied by oblique-texture electron-diffraction. Clay Miner 19(2):177–193

Vantelon D et al (2003) Iron distribution in the octahedral sheet of dioctahedral smectites. An Fe K-edge X-ray absorption spectroscopy study. Phys Chem Miner 30(1):44–53

Westre TE et al (1997) A multiplet analysis of Fe K-edge 1s- > 3d pre-edge features of iron complexes. J Am Chem Soc 119(27):6297–6314

Wilke M, Farges F, Petit P-E, Brown GE, Martin F (2001) Oxidation state and coordination of Fe in minerals: an Fe K-XANES spectroscopic study. Am Miner 86:714–730

Williams LB, Haydel SE, Ferrell RE (2009) Bentonite, bandaids, and borborygmi. Elements 5(2):99–104

Yang J et al (2012) Effects of redox cycling of iron in nontronite on reduction of technetium. Chem Geol 291:206–216

Journal : Large 269 | Dispatch : 7-8-2015 | Pages : 13
Article No : 768 | LE | TYPESET
MS Code : PCMI-D-15-00027 | CP | DISK